Predicting the electrical, mechanical, and geometric contributions to soft electroadhesives through fracture mechanics

Elayne M. Thomas,[a] Matthew K. McBride,[b+] Owen A. Lee,[b+] Ryan C. Hayward,[b]* and Alfred J. Crosby [a]*

[a] Department of Polymer Science and Engineering, University of Massachusetts Amherst, MA 01003, USA

[b] Department of Chemical and Biological Engineering, University of Colorado Boulder, CO 80303, USA

*Email: ryan.hayward@colorado.edu
*Email: acrosby@umass.edu

[+] *M.K.M and O.A.L contributed equally to this paper*

Keywords: Electroadhesion, soft electroadhesives, fracture mechanics, geometric confinement, ionoelastomers

Abstract

Electroadhesion is the modulation of adhesive forces through electrostatic interactions and has potential applications in a number of next-generation technologies. Recent efforts have focused on using electroadhesion in soft robotics, haptics, and biointerfaces that often involve compliant materials and non-planar geometries. Current models for electroadhesion provide limited insight on other contributions that are known to influence adhesion performance, such as geometry and materials properties. This study presents a fracture mechanics framework for understanding electroadhesion that incorporates geometric and electrostatic contributions for soft electroadhesives. We demonstrate the validity of this model with two materials systems that exhibit disparate electroadhesive mechanisms, indicating that this formalism is applicable to a variety of electroadhesives. The results show the importance of material compliance and geometric confinement in enhancing electroadhesive performance and provide structure-property relationships for designing electroadhesive devices.

Introduction

Electroadhesion, the use of electrostatic interactions to modulate adhesive forces, holds significant potential for manufacturing and robotics applications. This mechanism has several benefits over other routes to switchable adhesion because it can operate in diverse environments without control-

intensive motors or energy-intensive pumps. Although electroadhesion has been used for electrostatic chucks and space exploration since the 1960s,[1,2] recent efforts have explored electroadhesion in technologies such as soft robotics,[3,4] haptics,[5] and biointerfaces[6] that often involve compliant materials, non-planar geometries, and rough surfaces. However, the principles originally developed for electroadhesion of rigid materials and device geometries have limited relevance for these non-ideal surfaces, creating a need for new models to describe next-generation soft electroadhesive technologies.

Prior efforts to describe electroadhesion, particularly focusing on hard materials, has resulted in the development of both numerical and analytical models. Numerical models often require assumptions about surface roughness and sometimes neglect intrinsic van der Waals interactions, making them of limited utility for soft, viscoelastic materials.[7,8] Analytical models typically focus solely on maximum adhesion force or adhesion pressure, which provides limited insight enabling generalization to other materials systems, geometries, or failure modes.[3,9,10] Predictive models for electroadhesion that are generalizable to multiple materials systems must therefore incorporate other contributions that are known to influence adhesion performance, such as geometry and materials properties.

One approach to address this gap in understanding is to use fracture mechanics, a formalism that fully describes the mechanical and surface roles in adhesion and allows for translatable design rules between materials systems. Rather than force or pressure being the figure of merit for electroadhesion, adhesion is quantified by the energy per unit area required for interfacial separation.[11,12] This energy balance approach has been extensively used in the fracture mechanics community to describe adhesion and failure in soft elastomers, as the molecular forces at the interface that promote adhesion can be deconvoluted from dissipative phenomena within the material that slow the debonding process.

A notable finding from this approach is the importance of compliance in adhesion, where decreasing the thickness of the material increases its effective stiffness and enhances its adherence, or maximum separation force from a substrate. These compliance effects were previously rationalized using a confinement parameter a/h, where a is the interfacial length and h is the material thickness.[13] The importance of geometry was recently demonstrated for electrostatic clutches,[14] where the performance of the clutch was enhanced over 60-fold when the geometry was optimized, compared to other state-of-the-art devices. These influence of confinement, along with parameters like the Young's modulus, are critical to place in context with adhesion from electrostatic interactions, particularly in soft materials where the intrinsic adhesion is not negligible.

Here, we present a fracture mechanics framework for understanding electroadhesion that captures geometric and electrostatic contributions for contact adhesion in soft and hard electroadhesives.

We posit that electroadhesion acts as an added surface energy that opposes the mechanical and potential energy that drive delamination, which is validated with two soft materials systems with disparate electroadhesive mechanisms. We find that dissipative phenomena that slow the debonding processes contribute a multiplicative factor to enhance electroadhesive interactions at the interface. We further demonstrate and quantitatively describe how geometric confinement, or the ratio of interfacial length to thickness, can be used to control electroadhesion performance. Collectively, these results provide important structure-property relationships to design electroadhesive devices for specific applications in industrial and commercial settings.

2. Results and Discussion

2.1 Describing electroadhesion with fracture mechanics

We quantify the electrostatic and mechanical contributions to electroadhesion between two materials through the energy per unit area required to separate them. In this formalism, the interface between two materials in contact is defined by an interfacial area A, the periphery of which is viewed as a crack. As the area changes during interface formation and separation, the change in the total energy of the system (U_T) with respect to area is written as

$$\frac{dU_T}{dA} = \frac{dU_E}{dA} + \frac{dU_M}{dA} + \frac{dU_S}{dA} \qquad \text{Eq. 1}$$

U_E is the elastic (strain) energy stored in the material from deformation, U_M is the mechanical work from moving a load through a distance, and U_S is the surface energy of contact.[11] For this work, we posit that electroadhesion acts as an added surface energy, such that dU_S/dA contains both energy from intrinsic van der Waals interactions (w) and energy from electrostatic interactions:

$$\frac{dU_S}{dA} = -(w + \mu) \qquad \text{Eq. 2}$$

where μ is the change in electrostatic energy with respect to area. The negative sign is the result of a sign convention so that the surface energy increases with decreasing interfacial area.

As interfacial area decreases during debonding, the strain and mechanical energy available in the system decreases, indicating that the first two terms in Equation 1 will always favor delamination. The energy release rate, G, defines the change in elastic and mechanical energy for a given change in A:

$$G = \frac{dU_E}{dA} + \frac{dU_M}{dA} \qquad \text{Eq. 3}$$

The energy release rate can be viewed as the driving force for crack extension and removal of an interface between materials. The surface energy gained from the creation of new interface as the

crack propagates acts in opposition to these driving forces. Substituting Equations 2 and 3 into Equation 1 yields

$$\frac{dU_T}{dA} = G - (w + \mu) \qquad \text{Eq. 4}$$

Thus, crack propagation is favorable ($dU_T/dA > 0$) when the energy release rate overcomes both the intrinsic and electrostatic contributions to the surface energy. The lowest value of G that initiates debonding is known as the critical energy release rate, G_c. The term $G - w$ is often described as the "motive" that drives two materials in contact to separate; in the case of electroadhesion, μ acts as an additional, electric field-dependent resistance to separation. Since the energy release rate is obtained experimentally, the driving force for interface formation and separation can be determined throughout the entire measurement to obtain a fuller picture of how electroadhesion impacts the adhesion properties of materials. G is determined experimentally as a function of compliance (S), interfacial radius (a), and force (F):

$$G = -\frac{(F' - F)^2}{4\pi a} * \frac{dS}{dA} \qquad \text{Eq. 5}$$

where F' is the force in the absence of adhesion and A is the axisymmetric interfacial area.[15] The compliance depends both on the materials properties (Young's modulus E, and Poisson's ratio, v) and the degree of confinement, a/h. Previous work described a corrected form of compliance for hard on soft interfaces; more recently, an expression defining compliance for soft-soft interfaces was described.[16] More details can be found in the Supporting information.

Any inelastic processes within the contacting materials (such as polymer relaxation) dissipates energy and slow crack propagation, which affects the energy release rate. These energetic losses depend on the speed of the crack front (v) and have empirically been modeled by Gent and Shultz[17] as:

$$G_c = G_0 \left(1 + \left(\frac{v}{v*}\right)^n\right) \qquad \text{Eq. 6}$$

where n, the crack velocity exponent, describes the shape of the G_c versus v curve, $v*$ defines the crack velocity above which dissipative processes become prevalent in crack propagation, and G_0 is the threshold energy release rate for the onset of interface separation. Typically, n is between 0.3 and 1 for polymers.[13,18] Quantifying the velocity-dependent contributions to adhesion separately from the thermodynamic driving force enables us to describe the interfacial and bulk processes that affect how materials separate, which can more clearly define relevant structure-property relationships and strategize how materials systems can be designed to maximize performance.

2.2 Two materials systems with disparate electroadhesion mechanisms are used for experimental corroboration

To test the validity of this model, two materials systems that exhibit electroadhesion through different mechanisms are used in this work. Crosslinked polydimethylsiloxane (PDMS) (Figure 1a) is a material used for conventional electroadhesives that exhibits electroadhesion through dielectric polarization in response to an applied electric field. The derivative of the electrostatic energy (U_{EL}) with respect to area A for conventional electroadhesives is

$$\frac{dU_{EL}}{dA} = \frac{\frac{1}{2}\varepsilon\varepsilon_0 V^2}{d} = \frac{1}{2}CV^2 \qquad \text{Eq. 7}$$

where V is the applied voltage, d is the thickness of the material, ε is the dielectric constant, ε_0 is the dielectric permittivity in free space, and C is the capacitance of the material. Since PDMS has a dielectric constant of 2-3,[19] high electric fields are typically required to store significant amounts of electrostatic energy within the material.

The second system used in this study is a set of ionically-conducting elastomers (ionoelastomers) that rely on the motion of ions to exhibit electric field-enhanced adhesion. Ionoelastomers contain two types of ions: one type (either anion or cation) is covalently bound to the polymeric network, while the other is an untethered counterion (Figure 1a). This structure leads to an asymmetry in ion drift; mobile counterions quickly rearrange in the presence of an electric field, while bound ions do not drift. It was shown in previous work that two ionoelastomers in series, one with the cation covalently tethered (polycation) and one with the anion covalently attached (polyanion), can operate as an ionic diode due to the difference in polarity of the tethered ion.[20] In the polycation/polyanion diode, positive voltages ('forward' bias) forced mobile ions to drift across the interface, resulting in potential drop existing primary across the electrodes. With negative voltages ('reverse' bias), the covalently bound ions form an ionic double layer (IDL) across the polyanion/polycation interface, stopping the flow of current across the device.[20]

This ionoelastomer diode configuration was found to exhibit significant enhancement in adhesion force capacity in reverse bias.[21] This effect is not observed for two ionoelastomers with the same bound ion. As mobile ions move toward the electrodes in reverse bias, the interactions at the IDL leads to electric field-induced adhesion. The authors also employed high surface area electrodes to maximize the potential drop across the IDL, leading to a larger enhancement in adhesion for a given applied voltage. The nanometer-scale thickness of the IDL resulted in substantial enhancements in adhesion with potentials of less than 2 V. The derivative of the electrostatic energy (U_E) with respect to area A for the ionoelastomers is

$$\frac{dU_{EL,ionoelastomer}}{dA} = \mu_{ionoelastomers} = \frac{\frac{1}{2}\varepsilon\varepsilon_0 (V_B - V)^2}{d} = \frac{1}{2}C(V_B - V)^2 \qquad \text{Eq. 8}$$

where V_B is the built-in potential resulting from the distribution of ions at open circuit conditions, and C is the area-normalized capacitance of the IDL.[21] One added advantage of the ionoelastomers is that the thickness of the IDL is independent of bulk thickness, enabling a straightforward method to decouple geometric and electrostatic effects in electroadhesion.

To test the validity of our model, experiments are performed on a custom-built instrument to collect force, displacement, and interfacial area simultaneously, as shown schematically in Figure 1b. The force-displacement data in conjunction with interfacial area images (Figure 1c) were collected and used to calculate the elastic modulus and the critical energy release rate (G_c) as a function of voltage and geometry. Fitting the velocity dependence on G_c enables us to describe how the materials properties, geometry, and electrostatic interactions individually contribute to adhesion to create design rules for next-generation adhesive devices.

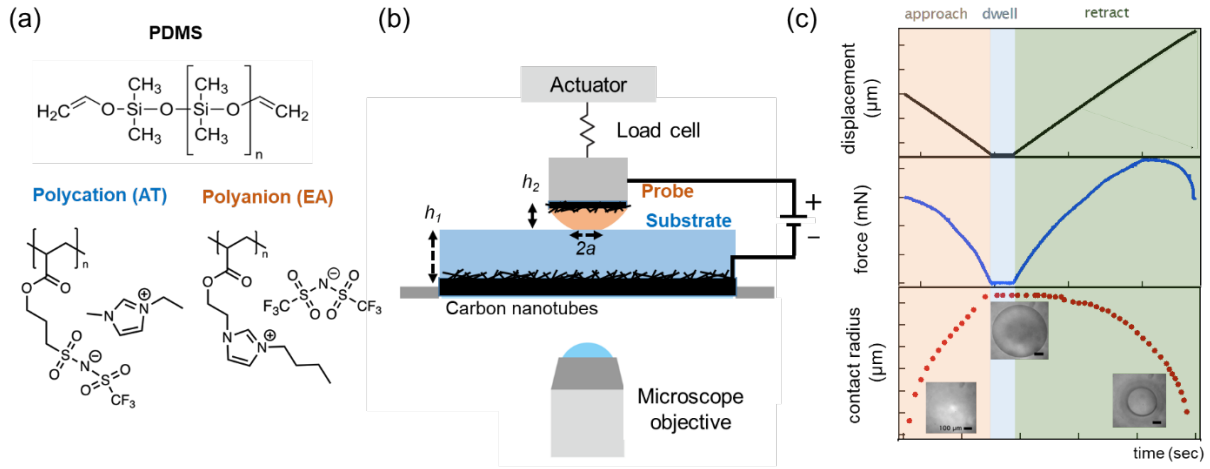

Figure 1. (a) Materials used in this work. PDMS is used as an electroadhesive whose dipoles rearrange in response to an electric field, while the ionoelastomers EA and AT utilize ion motion for electrically-modulated adhesion. (b) Experimental setup for electroadhesion experiments; h_1, h_2, and a correspond to the parameters used to define geometric confinement. (c) Example data for electroadhesion experiments. Force, displacement, and interfacial area are recorded simultaneously.

2.3 Ionoelastomers exhibit geometry- and capacitance dependent electroadhesion

Since the thickness of the IDL is independent of the thickness of the ionoelastomer networks, they act as an ideal system to decouple the geometric contributions from the strength of electrostatic interactions on adhesion as a function of voltage. Two networks were used for this work: a polyanion (EA) and polycation (AT), shown in Figure 1a. We tested samples of ionoelastomers in a hemisphere on flat geometry using two geometries: one sample with a smaller confinement ratio, a/h (denoted "low geometric confinement") and one sample with a larger confinement ratio

(denoted "high geometric confinement"). The confinement ratio of each component is defined separately as a/h_1 (for AT) and a/h_2 (for EA). In the results below, low geometric confinement refers to a/h_1:a/h_2 = 0.29:1.47, and high geometric confinement refers to a/h_1:a/h_2 = 0.70:2.23.

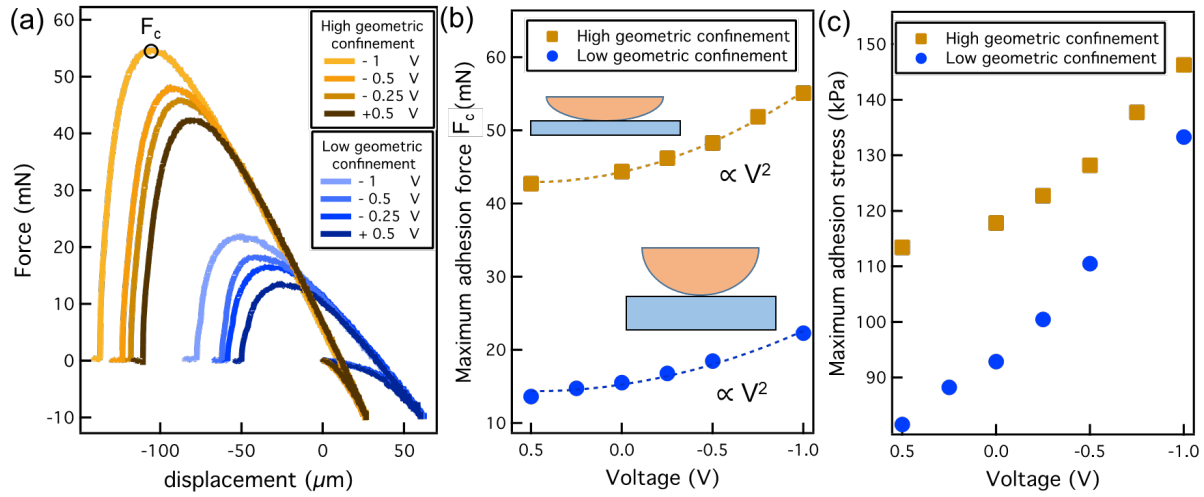

Figure 2. Enhancement in adhesion from ion conduction. (a) Force-displacement curves of two geometries tested: one pair that is highly confined geometry (brown curves), and one pair in a less confined geometry (blue curves). Although they are the same materials system, geometry plays a significant role in their maximum adhesion force, F_c. Both material pairs follow a quadratic relationship between voltage and (b) adhesion force and (c) adhesion stress, but the differences in geometry prevent the curves from collapsing on the same plot.

Geometric confinement influences both the peak adhesion force (F_c) of ionoelastomer heterojunctions and how F_c evolves with electric field, signifying that F_c alone is not a sufficient metric to describe electroadhesion. Each ionoelastomer sample is tested over a range of voltages from + 0.5 V to – 1 V, whose force-displacement curves are shown in Figure 2a. For a smaller confinement ratio (a/h_1:a/h_2 = 0.29:1.47, blue curves), F_c increases from 15 mN to 22 mN between + 0.5 V and – 1 V (Figure 2b) as a result of IDL formation in reverse bias. From chronoamperometry measurements, we find that the open-circuit potential of the heterojunction is approximately + 0.25 V (Supporting Information), consistent with previous work on similar ionoelastomers. Increasing the confinement ratio to a/h_1:a/h_2 = 0.70:2.23 (Figure 2a, brown curves) leads to a concomitant increase in F_c for all voltages, even when the IDL is not apparent. The increase in F_c with voltage follows a quadratic relationship from the traces in Figure 2b, consistent with previous electroadhesion literature.[9,10,21] However, the slope of the quadratic fit is not equivalent for the two samples even when normalized by maximum interfacial area (Figure 2c), despite electroadhesion occurring *via* the same mechanism. Since both samples have the same Young's modulus ($E \approx 800$ kPa), the discrepancy between the adhesion performances indicates that geometric confinement along with electrostatic interactions plays a significant role in determining how materials adhere.

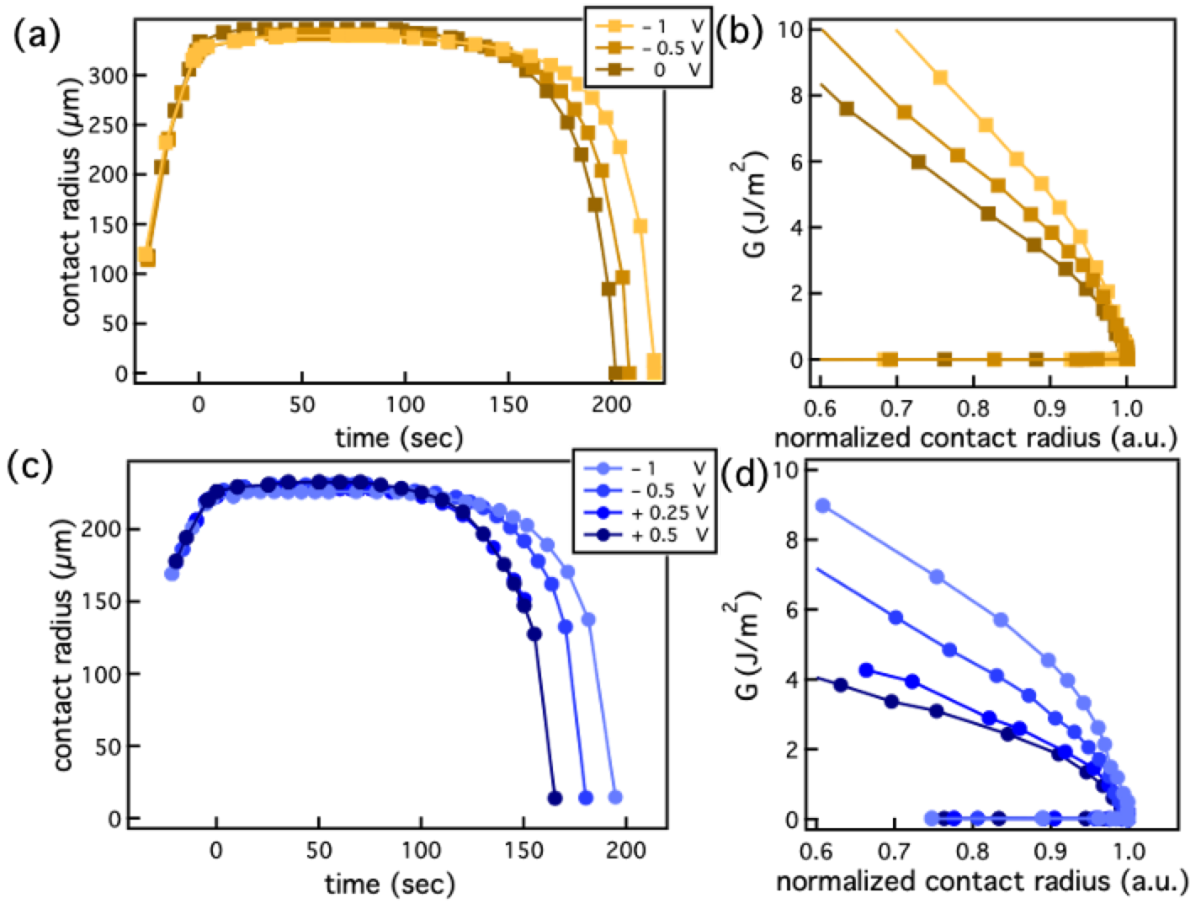

Figure 3. Interfacial contact radius and energy release rate, G, for samples with high (a,b) and low (c,d) geometric confinement. Increasing the bias toward negative values forms a stronger ionic double layer, increasing how long the ionoelastomers remain in contact.

Interfacial area measurements reveal that the formation of an IDL between AT and EA extends the time that the ionoelastomers remain in contact, which is indicative of an increased driving force necessary for crack propagation (Figure 3). Representative plots of each confinement geometry show that with increasing compressive force, the interfacial radius of the heterojunction increases until the maximum compressive force is reached (denoted as time = 0 s indicated by Figure 3a and Figure 3c). During the dwell time to charge the IDL, there is some stress relaxation where the interfacial radius increases by < 5%. During retraction, interactions at the interface oppose the strain and mechanical energy that increase as the heterojunction is pulled in tension. Interfacial area begins to decrease as the G exceeds G_c; eventually, complete separation occurs. Independent of geometry, higher reverse-biases strengthens the electrostatic interactions at the EA/AT interface, which necessitates higher values of strain energy for the onset of delamination at the same interfacial radius (Figure 3b and Figure 3d). These results suggest that G_c is dependent on the capacitive contributions; however, it is unclear whether the electroadhesion acts purely at the interface or has additional roles during the delamination process.

2.4 Electroadhesion manifests in the thermodynamic contribution to G_c

Separating G into thermodynamic and dissipative contributions helps to delineate the purely interfacial interactions from bulk processes that affect adhesion. For most soft materials, some component of the strain energy that is stored into the interfacial area is not perfectly transferred into energy to create new surfaces; some fraction is lost as heat that is absorbed into the material near the crack tip. The amount of energy lost as heat increases as the propagation speed increases. Therefore, Equation 6 is used to deconvolute purely interfacial interactions from inelastic phenomena that influence G_c.

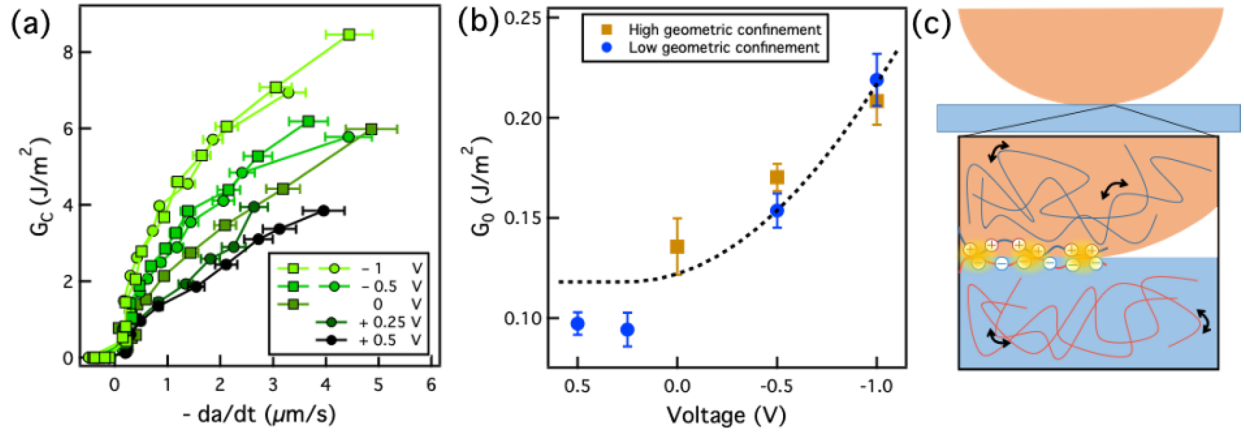

Figure 4. Accounting for differences in geometric confinement between ionoelastomers using a fracture mechanics approach leads to the collapse of the energy release rate with voltage. (a) G_c as a function of crack velocity, $-da/dt$. Horizontal error bars are a result of error in crack velocity calculations. For all ionoelastomer experiments, greater values of reverse bias increase the energy release rate as a function of crack propagation and fall within error for the same values of voltage. (b) The work of adhesion collapses on a master curve as defined by Equation 10. (c) A schematic for the electroadhesion mechanism of ionoelastomers. Both the electrostatic interactions at the interface along with viscoelastic relaxation processes contribute to electroadhesion, and can be decoupled using a fracture mechanics analysis.

The electrostatic interactions at the ionoelastomer interface mainly influence the thermodynamic energy release rate and are geometry-independent, with the inelastic contributions acting as a multiplicative factor in the strain energy required to separate an interface. Figure 4a shows G_c as a function of crack velocity v (calculated as the negative change in interfacial radius as a function of time, $-da/dt$) for both confinement geometries. As expected from Figure 3a and 3c, increasingly negative voltages (reverse bias) lead to increased G_c for the same crack velocity, da/dt. We also find that samples with different confinement geometry collapse on the G_c versus v plot, indicating that our model captures the geometric as well as the capacitive components of electroadhesion. Fitting G_0 for each curve in Figure 4a using Equation 6 ($v^* = 20$ nm/s, $n = 0.6$) shows that G_0

follows a quadratic dependence with voltage (Figure 4b). From Eq. 4, we infer that G_0 should take the form

$$G_0 = \mu + w = \frac{1}{2}C(V_B - V)^2 + w \qquad \text{Eq. 9}$$

With the built-in potential from the ionoelastomers being +0.25 V, in agreement with chronoamperometry (Figure S2) and similar to previous work, fitting the G_0 data in Figure 4a leads to the work of adhesion w = 0.11 J/m^2, which is comparable to other acrylate-based elastomer interfaces.[13,22] Additionally, we find from the fit that the capacitance of the ionic double layer, C_{IDL}, is 12 μF/cm^2. This value is of similar magnitude to those for planar interfaces of other electrolytes, although it is an order of magnitude larger than previously measured by ac impedance spectroscopy for a similar ionoelastomer heterojunction.[21] Although the reason for this discrepancy is not completely clear, one possible explanation is that the structure of the IDL evolves with applied bias (i.e., the degree of interpenetration of the networks increases under reverse bias), leading to a stronger effect on adhesion than estimated based on capacitance alone.

The full form for G_c with electroadhesion by combining Equations 6 and 9 is

$$G_c = \left(\frac{1}{2}C(V_B - V)^2 + w\right) * \left(1 + \left(\frac{v}{v*}\right)^n\right) \qquad \text{Eq. 10}$$

Although the capacitive effects at the interface only influence the thermodynamic limit of G_c, these influences have a multiplicative effect at non-zero velocities, where the inelastic processes that dissipate energy at the crack front (defined by v*) determine the magnitude of adhesion enhancement at a given separation velocity (Figure 4c). By providing a full description of the interplay of factors that influence electroadhesion, this framework enables rational development of a material or device depending on the design requirements of a specific end use.

2.5 Our framework also captures the behavior of conventional dielectric electroadhesives

In addition to the ionoelastomers, our model successfully describes the operation of PDMS-based dielectric electroadhesives. Here, we use a crosslinked PDMS network diluted with linear PDMS to maintain an elastic character while maintaining a low modulus (E = 18.5 kPa). Voltage was applied at a maximum compressive force of 25 mN and maintained until the end of the experiment.

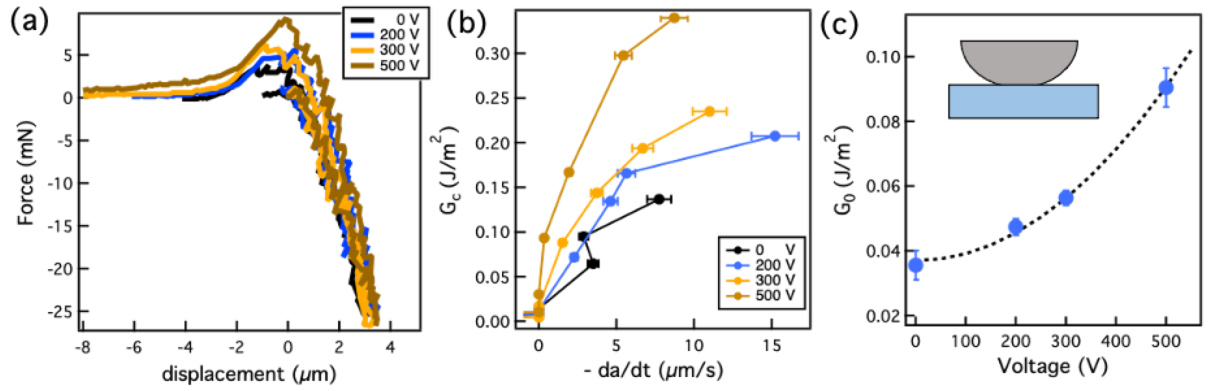

Figure 5. Electroadhesion with a conventional elastomer. Higher voltages are required for an observable increase in F_c (a), but our approach yields reasonable values for G_c (b) and G_0 (c) as a function of voltage.

Similar to the ionoelastomers, the force capacity of the interfaces between the PDMS film (h = 22 μm) and a stainless steel probe increases with an increased applied voltage (Figure 5a); however, the low dielectric constant of PDMS requires higher electric fields for an observable enhancement in adhesion. The high electric fields also lead to a capacitive "tail" in the force-displacement curves after the material comes out of interfacial contact. Increasing the applied voltage from 0 V to 500 V leads to an increase in force capacity from 3 to 8 mN. The trend in interfacial radius with voltage is consistent with the ionoelastomers (Figure S3), where higher voltage leads to an extended interfacial time prior to separation. The high confinement ratio (a/h = 10) results in the formation of a mechanical instability, after which the interfacial radius becomes non-circular and invalidates the use of Equation 5. Although the non-circular, or "fingering," instability limits the interfacial radius data, we can apply our model until the instability occurs.

Capacitive contributions to electroadhesion are primarily in the thermodynamic work of adhesion with PDMS, where a more elastic system limits the enhancement of adhesion performance at higher velocities. Similar to the ionoelastomers, we observe a clear increase in G_c for a given crack velocity with higher voltages (Figure 5b); fitting Equation 10 (V_B = 0 for PDMS) for each voltage leads to a quadratic dependence on G_0 with voltage for a constant v^* (v^* = 662 nm/s, n = 0.5) (Figure 5c). The higher value of v^* compared to the ionoelastomers arises from the significantly greater elastic character of the material. From the quadratic fit, we find that the y-intercept w = 0.04 J/m^2 and C = 430 nF/m^2 for the PDMS film. While these fitting parameters are slightly lower than typical values for w and C of PDMS on steel based on literature values (w = 0.05 - 0.1 J/m^2, C = 800 nF/m^2 for h = 22 μm, ε = 2),[19,23] the ability to capture the behavior of two different soft systems with very reasonable parameters provides strong validation to our proposed model and its implications for electroadhesive design. As the areal capacitance of the PDMS elastomer will change with thickness, we expect a different slope if a different value of h is used; however, these results indicate that our model accurately captures each contributing factor to electroadhesion to enable the design of a device for a given performance.

An interesting observation in the PDMS system worth noting here is the evolution of interfacial morphology during delamination with voltage. Due to the high confinement ratio, the lateral stresses in the film are released by the formation of finger-like features around the center of the interfacial area. We find that while the primary wavelength is independent of the electric field, the amplitude of the fingers that form prior to delamination increases with applied voltage, as evidenced by interfacial images taken at 70% of the maximum tensile strain before complete separation (Figure S4). This observation is reminiscent of electrohydrodynamic instabilities studied in polymer melts and later in films;[24,25] understanding the interaction between instabilities as a result of geometric confinement and applied electric fields will provide interesting opportunities for switchable and shape-morphing materials.

Conclusion

This work provides a unifying framework to describe the multitude of contributions to electroadhesion. Through two disparate soft materials systems, we find that using an energy balance to account for the capacitive effects enabled through electroadhesion, in conjunction with the mechanical and materials contributions, is critical to understand the design principles of soft electroadhesives. By rationalizing the scaling of crucial design criteria such as material thickness, operating voltage, dielectric constant, and elastic modulus, an electroadhesive device can be developed to meet adhesion specifications through multiple design pathways. We posit that this formalism is general for any soft materials system and can be used if the capacitance, elastic modulus, and geometric constraints are known. Our results carry significant weight for applications in soft robotics, neural interfacing, and medical devices to create novel materials and device geometries for a specific end use.

There are several exciting new opportunities uncovered by this work. While this configuration is relevant to many applications such as closures, many other applications use more complicated electrode geometries. Extending this model for more complex electrode configurations will provide useful guidance in a wider variety of devices. Additionally, while we used this model for rationalizing electrostatic interactions, we expect this formalism to hold for other switchable interfacial phenomena whose energy has a closed form, such as magnetic or light-responsive interactions. Lastly, while we observed some changes in delamination morphology for the PDMS films, we did not observe a transition between separation modes with increasing electric field. Exerting control over the primary failure mode in adhesion is useful for energy management and repeatability. Increasing the velocity at which the experiment is run will increase the enhancement in G_c from electroadhesion, which may lead to an electric field-induced transition between failure modes. Additionally, since our formalism is based in contact mechanics, the model describes adhesion only in the region where the two materials are in contact. However, especially in the case of the dielectric electroadhesive system, interactions outside of the contact region can play a non-

negligible role; including corrections due to non-contact interactions is an important subject for future work.

Supporting Information: Synthesis of EA, chronoamperometry results, and additional details of PDMS electroadhesion analysis, including images of contact instabilities (PDF)

Acknowledgements

This work is supported in part by the US Army Research Laboratory and the US Army Research Office under grant W911NF-15-1-0358. Monomer and polymer synthesis were supported by the National Science Foundation under grant EFRI-1935294. We thank Professor Hyeong Jun Kim for insightful discussions. We thank Professor Tom Russell for the use of the high-voltage source.

References

(1) Krape, R. P. *Applications Study of Electroadhesive Devices*; NASA-CR-1211; 1968. https://ntrs.nasa.gov/citations/19680028434 (accessed 2022-02-09).

(2) McGinty, G. K. Semiconductor Device Manufacture. US3993509A, November 23, 1976. https://patents.google.com/patent/US3993509A/en?oq=McGinty+GK+(1976)+Semiconductor+device+manufacture.+US+Patent+3%2c993%2c509 (accessed 2022-02-09).

(3) Gu, G.; Zou, J.; Zhao, R.; Zhao, X.; Zhu, X. Soft Wall-Climbing Robots. *Science Robotics* **2018**, *3* (25). https://doi.org/10.1126/scirobotics.aat2874.

(4) de Rivaz, S. D.; Goldberg, B.; Doshi, N.; Jayaram, K.; Zhou, J.; Wood, R. J. Inverted and Vertical Climbing of a Quadrupedal Microrobot Using Electroadhesion. *Science Robotics* **2018**, *3* (25), eaau3038. https://doi.org/10.1126/scirobotics.aau3038.

(5) Hinchet, R.; Shea, H. High Force Density Textile Electrostatic Clutch. *Advanced Materials Technologies* **2020**, *5* (4), 1900895. https://doi.org/10.1002/admt.201900895.

(6) Borden, L. K.; Gargava, A.; Raghavan, S. R. Reversible Electroadhesion of Hydrogels to Animal Tissues for Suture-Less Repair of Cuts or Tears. *Nat Commun* **2021**, *12* (1), 4419. https://doi.org/10.1038/s41467-021-24022-x.

(7) Persson, B. N. J.; Guo, J. Electroadhesion for Soft Adhesive Pads and Robotics: Theory and Numerical Results. *Soft Matter* **2019**, *15* (40), 8032–8039. https://doi.org/10.1039/C9SM01560D.

(8) Bigharaz, M.; Schenkel, T.; Bingham, P. A. Increasing Force Generation in Electroadhesive Devices through Modelling of Novel Electrode Geometries. *Journal of Electrostatics* **2021**, *109*, 103540. https://doi.org/10.1016/j.elstat.2020.103540.

(9) Chen, A. S.; Bergbreiter, S. A Comparison of Critical Shear Force in Low-Voltage, All-Polymer Electroadhesives to a Basic Friction Model. *Smart Mater. Struct.* **2017**, *26* (2), 025028. https://doi.org/10.1088/1361-665X/aa5484.

(10) Guo, J.; Leng, J.; Rossiter, J. Electroadhesion Technologies for Robotics: A Comprehensive Review. *IEEE Transactions on Robotics* **2020**, *36* (2), 313–327. https://doi.org/10.1109/TRO.2019.2956869.
(11) Maugis, D.; Barquins, M. Fracture Mechanics and the Adherence of Viscoelastic Bodies. *J. Phys. D: Appl. Phys.* **1978**, *11* (14), 1989–2023. https://doi.org/10.1088/0022-3727/11/14/011.
(12) Johnson, K. L.; Kendall, K.; Roberts, A. D. Surface Energy and the Contact of Elastic Solids. *Proceedings of the Royal Society of London. Series A, Mathematical and Physical Sciences* **1971**, *324* (1558), 301–313.
(13) Shull, K. R.; Ahn, D.; Chen, W.-L.; Flanigan, C. M.; Crosby, A. J. Axisymmetric Adhesion Tests of Soft Materials. *Macromolecular Chemistry and Physics* **1998**, *199* (4), 489–511. https://doi.org/10.1002/(SICI)1521-3935(19980401)199:4<489::AID-MACP489>3.0.CO;2-A.
(14) Levine, D. J.; Iyer, G. M.; Daelan Roosa, R.; Turner, K. T.; Pikul, J. H. A Mechanics-Based Approach to Realize High-Force Capacity Electroadhesives for Robots. *Sci Robot* **2022**, *7* (72), eabo2179. https://doi.org/10.1126/scirobotics.abo2179.
(15) Shull, K. R. Contact Mechanics and the Adhesion of Soft Solids. *Materials Science and Engineering: R: Reports* **2002**, *36* (1), 1–45. https://doi.org/10.1016/S0927-796X(01)00039-0.
(16) Thomas, E. M.; Fu, H.; Hayward, R. C.; Crosby, A. J. Geometry-Controlled Instabilities for Soft–Soft Adhesive Interfaces. *Soft Matter* **2022**, *18* (42), 8098–8105. https://doi.org/10.1039/D2SM00808D.
(17) Gent, A. N.; Schultz, J. Effect of Wetting Liquids on the Strength of Adhesion of Viscoelastic Material. *The Journal of Adhesion* **1972**, *3* (4), 281–294. https://doi.org/10.1080/00218467208072199.
(18) Zhang Newby, B.; Chaudhury, M. K. Friction in Adhesion. *Langmuir* **1998**, *14* (17), 4865–4872. https://doi.org/10.1021/la980290l.
(19) Kuo, A. C. M.; Mark, J. E. *Polymer Data Handbook,* 1st ed.; Oxford University Press, 1999; p. 411.
(20) Kim, H. J.; Chen, B.; Suo, Z.; Hayward, R. C. Ionoelastomer Junctions between Polymer Networks of Fixed Anions and Cations. *Science* **2020**, *367* (6479), 773-+. https://doi.org/10.1126/science.aay8467.
(21) Kim, H. J.; Paquin, L.; Barney, C. W.; So, S.; Chen, B.; Suo, Z.; Crosby, A. J.; Hayward, R. C. Low-Voltage Reversible Electroadhesion of Ionoelastomer Junctions. *Advanced Materials* **2020**, 2000600. https://doi.org/10.1002/adma.202000600.
(22) Mangipudi, V. S.; Tirrell, M. Contact-Mechanics-Based Studies of Adhesion between Polymers. *Rubber Chemistry and Technology* **1998**, *71* (3), 407–448. https://doi.org/10.5254/1.3538490.
(23) Nase, J.; Ramos, O.; Creton, C.; Lindner, A. Debonding Energy of PDMS. *Eur. Phys. J. E* **2013**, *36* (9), 103. https://doi.org/10.1140/epje/i2013-13103-3.

(24) Schäffer, E.; Thurn-Albrecht, T.; Russell, T. P.; Steiner, U. Electrically Induced Structure Formation and Pattern Transfer. *Nature* **2000**, *403* (6772), 874–877. https://doi.org/10.1038/35002540.
(25) Schäffer, E.; Thurn-Albrecht, T.; Russell, T. P.; Steiner, U. Electrohydrodynamic Instabilities in Polymer Films. *EPL* **2001**, *53* (4), 518. https://doi.org/10.1209/epl/i2001-00183-2.
(26) Lee, O. A.; Ticknor, M.; McBride, M. K.; Hayward, R. C. Pendent Sulfonylimide Ionic Liquid Monomers and Ionoelastomers via "SuFEx" Click Chemistry. Submitted. **2023**.
(27) Chan, E. P.; Smith, E. J.; Hayward, R. C.; Crosby, A. J. Surface Wrinkles for Smart Adhesion. *Advanced Materials* **2008**, *20* (4), 711–716. https://doi.org/10.1002/adma.200701530.

Experimental

Materials. 1–[2–Acryloyloxyethyl]–3–buthylimidazolium] bis(trifluoromethane) sulfonimide (AT) was synthesized as detailed in a previous publication.[21] 1-ethyl-3-methylimidazolium 3-sulfonyl(trifluoromethane sulfonyl) imide propyl acrylate (EA) was synthesized as described elsewhere,[26] and summarized in the Supporting Information. Poly(ethylene glycol) diacrylate (PEGDA) was purchased from Sigma-Aldrich and used as received. 2,2-Dimethoxy-2-phenylacetophenone (DMPA) was purchased from Sigma-Aldrich and used as received. Poly(dimethyl siloxane) elastomer (PDMS) was prepared from a Sylgard™184 kit obtained from Dow Corning. Methyl-terminated linear PDMS (LPDMS) was obtained from Gelest (13.5 kg/mol) and used as received. Single-walled carbon nanotube (CNT) conductive ink was purchased from Sigma-Aldrich (1.00 mg/mL, 791504-25 mL) and diluted to 0.5 mg/mL with DI water before use. 3-(Trimethoxysilyl) propyl methacrylate was purchased from Sigma-Aldrich (M6514) and used as received. ITO-coated glass substrates were purchased from University Wafer. All solvents were used as received.

Carbon nanotube-coated substrate preparation. A solution of single-walled CNTs (diluted to 0.5 mg/mL) was subjected to horn sonication (Qsonica) for 15 min. Glass substrates were cleaned with UV-ozone for 15 min. A solution of 3-(trimethoxysilyl) propyl methacrylate (8 wt % in acetone) was dropcast on the substrates to act as an adhesion promoter. Coated substrates were placed on a hotplate at 180 °C, and the CNT solution was spray-coated using a commercial air brush (Iwata Eclipse HP-CS) from a distance of 15 cm at a pressure of 20 psi. The CNT solution (5 mL) was sprayed which resulted in a sheet resistance of 480 ± 137 Ω/sq.

Ionoelastomer sample preparation. Monomer solutions of EA and AT were made by vigorously mixing monomer, 5 mol% of PEGDA, and 1 mol% of DMPA (200 mg/mL in acetonitrile). For substrate samples, the monomer solution was dropcast onto carbon nanotube glass slides in a rectangular PDMS well. For the hemispherical probe samples, monomer solution was dropcast onto a CNT-coated glass substrate in a circular PDMS well with diameter 2 mm, 3 mm, or 4 mm to govern the curvature of the hemisphere. Dropcast samples were crosslinked under UV light (Nailstar Professional 12W LED lamp) for 30 min in a nitrogen atmosphere. Polymerized samples

were washed in a 50/50 mixture by volume of dichloromethane and isopropanol for 48 h to extract unreacted monomer, changing solvent after 24 hours. After extraction, samples were annealed at 80 °C for 12 h under vacuum (1 Torr) to remove residual solvent before use.

PDMS sample preparation. The PDMS prepolymer and curing agent were first pre-mixed with a 30:1 ratio of prepolymer to curing agent by weight. The mixture was diluted to a weight fraction of 0.7 with LPMS pre-cure to obtain the desired mechanical properties. The mixture was degassed for 30 minutes and cast onto ITO-coated glass substrates using a doctor blade (Qualtech QPI-FFT2) to control the thickness. The formulations were cured for 48 hours at 70 °C.

Interfacial adhesion tests. Adhesion measurements were performed on a custom-built instrument described in previous literature.[27] Briefly, displacement (δ) is controlled by a piezoelectric actuator (Burleigh Inchworm nanopositioner) and force (F) is measured using a capacitance-based load sensor (PI E-852 PISeca Signal Conditioner). For the ionoelastomer measurements, a probe made from AT is connected to a cantilever which deflects when in interfacial with the EA substrate, which is converted into a force. The load cell and actuator are mounted over an inverted microscope (Zeiss Axiovert 200M). For PDMS measurements, a metallic probe was connected to the cantilever. The adhesion measurements were performed by bringing the probe into interfacial with the substrate at a displacement rate of 1 μm/s until a maximum compressive preload. For ionoelastomers, there was an additional 60 s dwell time at the maximum compressive load for the ionic double layer to for. The probe was then retracted until complete separation occurred. Force, displacement, and interfacial area images were continuously collected with a custom Labview program during the experiment. For the ionoelastomers, voltage was applied and current recorded with a potentiostat (WaveNow, Pine Research Instrumentation), while voltage was applied with a high-voltage source (Matsusada Precision) for the PDMS measurements. Each experiment was analyzed with a custom MATLAB code to quantify adhesion performance.

Table of Contents (TOC) Figure